Available online at www.sciencedirect.com
SCIENCE DIRECT®
Robotics and Autonomous Systems 51 (2005) 297–310
Robotics and Autonomous Systems
www.elsevier.com/locate/robot

Introducing Climax: A novel strategy to a tri-wheel spiral robot

Amir Homayoun Javadi [a,*], Puyan Mojabi [b,1]

[a] *Azad University of Qazvin, Electrical and Computer Engineering Department, Navab Str., Azad University, P.O. Box 34197-416, Qazvin, Iran*
[b] *Iran University of Science and Technology, Electrical and Computer Engineering Department, No. 25, Resalat Str., Northern Naderi, Qazvin, Iran*

Received 12 November 2002; received in revised form 16 April 2004; accepted 16 May 2004
Available online 3 May 2005

Abstract

This paper describes a prototype and analytical studies of a tri-wheel spiral mobile robot. The robot can reach any desired point with a sequence of rotational movements. The robot has a simple actuation mechanism, consisting of three wheels mounted on a platform with axes fixed in 120° and a motor connected to each. Our approach introduces several new features such as simple repeated sequence of commands for steering and spiral motion, versus direct movement to target. The mathematical model of the robot is discussed, and a steering method is developed to achieve full motion capabilities. For a number of missions, it is shown experimentally that the proposed motion planning agrees well with the results.
© 2005 Elsevier B.V. All rights reserved.

Keywords: Spiral robot; Tri-wheel robot; Path planning

1. Introduction

We are in the process of development of a tri-wheel spiral mobile robot (nicknamed "Climax"), that has several new features than existing wheel- and track-based mobile robots. Our design is an isostatic structure equipped with three wheels located at the vertices of an equilateral triangle, with their axes pointing toward the center. The prototype of the robot is shown in Fig. 1. The actuation mechanism will provide the robot with rapid maneuverability by enabling it to quickly accelerate and decelerate, or move with constant velocity. One obvious feature of Climax is its natural spiral motion, versus direct movement, which brings us several advantageous properties as we will see in the following sections.

The outline of the paper is as following: introduction in Section 1; Section 2 is a glance on several specialized wheel and mobile mechanisms for constructing mobile robot; Section 3 shows a description of the system, and mathematical model of the robot; trajectory planning is brought in Section 4; Section 5 is devoted

* Corresponding author. Tel.: +98 281 222 9990; fax: +98 281 366 5279.
E-mail addresses: javadi@noise.ir (A.H. Javadi), mojabi@anoise.com (P. Mojabi).
[1] Tel.: +98 281 333 5685; fax: +98 281 334 5656.

0921-8890/$ – see front matter © 2005 Elsevier B.V. All rights reserved.
doi:10.1016/j.robot.2004.05.007

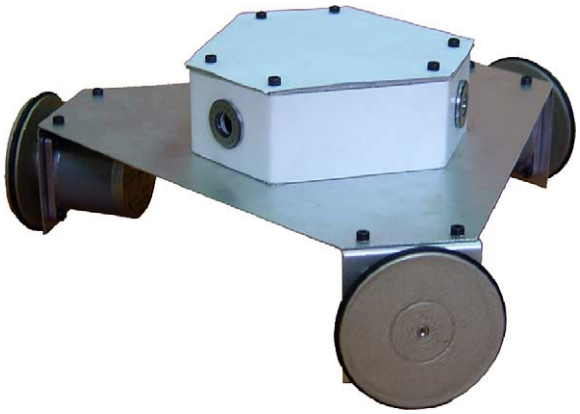

Fig. 1. Climax.

to experimental results; Section 6 gives an example of the advantageous of spiral motion; conclusion remarks in Section 7.

2. Flash back

A large number of wheeled or tracked platform mechanisms have been studied and developed to prove their mobility capability to tele-operate and/or to design autonomous robot vehicles [1]. For large and heavy outdoor robots, four-wheel car-like driving mechanisms or skid–steer platforms have traditionally been used. These vehicles are quite restricted in their motion [2–4], particularly when operating in tight environments, due to nonholonomic constraints on their wheel mechanisms. In recent years, study of nonholonomic systems is an area of active research. Nonholonomic systems are characterized by nonintegrable rate constraints resulting from rolling contact or momentum conservation. Nonholonomic behaviors are sometimes introduced on purpose in the design of mechanism, in order to obtain certain characteristics and performances such as those in [5–9]. Many applications fall into this category including wheeled robots, spacecrafts and underwater vehicles. Some elegant solutions to motion planning have been presented using tools from differential geometry [10–13]. One advantage offered by nonholonomic systems is the possibility of controlling a higher number of configurations than the number of actuators actually employed in the system, which is sometimes useful in terms of reducing the system's weight and cost [14]. The nonholonomic constraints cause complexities in trajectory planning and designing of control algorithms for feedback stability of the vehicle system. It is required that a suitable desired trajectory satisfying the above constraint be designed to control a nonholonomic mobile mechanism [15].

On the other hand, holonomic vehicles have been proposed with several advantages and disadvantages, so that there is introduced a control strategy to avoid a nonholonomic constraint of a wheel to implement a holonomic omnidirectional vehicle [16]. Holonomic vehicles, also, have some problems in practical applications such as low payload capability, complicated mechanism and limited accuracy of motion [17–19].

Better motion capabilities have been investigated in a variety of research centers and have been demonstrated on laboratory robots. These improvements in motion capabilities typically are derived from the use of two independent driving wheels supplemented by casters (e.g., see robot in [20]), two steerable and independently driving wheels [21] or three steerable and coordinated driving wheels (e.g., see robots in [22–24]). Some researchers, also, have developed spherical rolling robots [25–29] to achieve an omnidirectional motion [29].

The holonomic or nonholonomic omnidirectional mobile robots have been studied by using a variety of mechanisms [30,31]. In other words, several omnidirectional platforms have been known to be realized by developing a specialized wheel or mobile mechanism. From this point of view, such specialized mechanisms suitable for constructing an omnidirectional mobile robot are summarized as following:

1. Steered wheel mechanism [32].
2. Universal wheel mechanism [33].
3. Ball wheel mechanism [19,34].
4. Orthogonal wheel mechanism [18,34].
5. Crawler mechanism [35].
6. Offset steered wheel mechanism [16].

Our design, however, differs from previous works. Climax is a novel approach to a spiral mobile robot that introduces a new method of traveling. This approach has a simple mechanism and a good accuracy versus holonomic vehicles and further, it has no complexity in trajectory planning and designing of control algorithms. Moreover, it should have a rotary motion to move toward the target, which solely introduces sev-

eral new features such as providing full 360° view in the case of camera mounting and it can achieve a desired orientation easily than conventional mobile platforms. These features are achieved in the expense of wasting some energy as discussed in the following sections.

3. System description and mathematical model

Suppose that the robot is placed in the center of the O_m–X_mY_m coordinates, and one of the wheels is placed on the horizontal axis, X_m. Then, as the robot has an equilateral construction, and the axes of the other two wheels are placed in 120° with the axis of the first wheel, the position of the wheels will become as below:

$$\begin{aligned} x_1 &= r \\ x_2 &= x_3 = -\frac{1}{2}r \\ y_1 &= 0 \\ y_2 &= -y_3 = -\frac{\sqrt{3}}{2}r \end{aligned} \tag{1}$$

where r is the length of the vector connecting the center of the robot to the contacting point of the wheels, $\vec{v}_i$, and (x_i, y_i) (i = 1–3) are the respective contacting points of wheels in O_m–X_mY_m coordinates, as it is shown in Fig. 2.

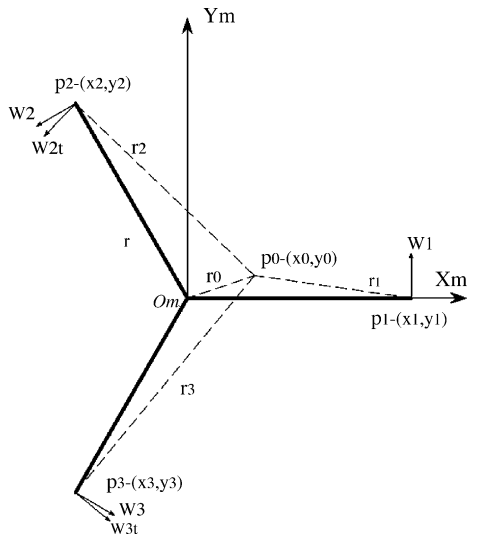

Fig. 2. The moving coordinates, O_m–X_mY_m, and the special alignment of the robot.

As far as the velocity of wheels is concerned, the body may be considered to be in pure rotation about an axis, normal to the plane of motion, passing through an axis. This axis is called the *instantaneous axis* of zero velocity, and the intersection of this axis with the plane of motion is known as the *instantaneous center* of zero velocity. This point is a unique reference point, p_0, which momentarily has zero velocity. As the angular velocity of wheels vary, p_0 changes. The point p_0 is, for our system as we have fixed wheels' axes, a fixed point in the body and a fixed point in the plane.

For the body in Fig. 2, let us assume that the directions of the absolute velocities of the any two wheels are known, suppose wheels 2 and 3, which certainly are not parallel. If there is a point about which p_2 has absolute circular motion at the instant considered, this point must lie on the normal to $\vec{w}_{2t}$ through p_2. Similar reasoning applies to p_3, and the intersection p_0 of these two perpendiculars fulfills the requirement for an absolute center of rotation at the instant considered. Point p_0 is the instantaneous center of zero velocity and may lie on or off the body. So, if $\vec{w}_i$ is the angular velocity of p_i, then $\vec{w}_{it}$, i = 1, . . ., 3, will become as below:

$$|\vec{w}_{it}| = |\vec{w}_i| \cos\theta_i \tag{2}$$

$$|\vec{w}_{in}| = |\vec{w}_i| \sin\theta_i \tag{3}$$

where θ_i is the angle between $\vec{v}_i$ and the vector connecting p_0 and p_i, $\vec{r}_i$. $\vec{w}_{in}$ is, also, the other decomposed vector of $\vec{w}_i$.

If the magnitude of the velocity of one of the wheels, say w_{2t}, is also known, the angular velocity w of the body and the linear velocity of every points in the body are easily obtained. Thus, the angular velocity of the body is:

$$w = \frac{w_{2t}}{r_2} \tag{4}$$

where r_2 is the distance between p_0 and p_2, and (4), of course, is also the angular velocity of every point in the body.

Therefore, the velocity of p_3 is $w_{3t} = r_3 w = (r_3/r_2)w_{2t}$. So the governing equation is as Eq. (5), which is a system of two equations and two variables, x_0 and y_0, the coordinates of p_0.

$$\frac{w_{1t}}{r_1} = \frac{w_{2t}}{r_2} = \frac{w_{3t}}{r_3} \tag{5}$$

$$\cos\theta_i = \frac{r_i^2 + r^2 - r_0^2}{2r_i r} = \frac{r^2 - (x_0x_i + y_0y_i)}{r_i r} \tag{6}$$

$$r = \sqrt{x_1^2 + y_1^2} = \sqrt{x_2^2 + y_2^2} = \sqrt{x_3^2 + y_3^2} \tag{7}$$

$$r_0 = \sqrt{x_0^2 + y_0^2} \tag{8}$$

$$r_i = \sqrt{(x_i - x_0)^2 + (y_i - y_0)^2} \tag{9}$$

and w_{it}, $i = 1, \ldots, 3$, are calculated using Eq. (2).

As the proposed system of Eq. (5) is a system of two biquadratic functions with two variables, there is no explicit solution for it. So we cannot develop constraints on wheel velocity since the solution is time consuming. Here, we introduce another system of equations which is simpler than (5) and needs less labor for solving.

Suppose that the wheels are rotating. It is evident that the wheel with higher speed should move in a longer radius. It means that the instantaneous center of zero velocity for the wheel with higher velocity should lie somewhere farther than the other wheels. So we have a system of equations as below:

$$\begin{cases} (x_0 - x_1)^2 + (y_0 - y_1)^2 = \left(\dfrac{k \cdot w_1}{w_1 w_2 w_3}\right)^2 \\ (x_0 - x_2)^2 + (y_0 - y_2)^2 = \left(\dfrac{k \cdot w_2}{w_1 w_2 w_3}\right)^2 \\ (x_0 - x_3)^2 + (y_0 - y_3)^2 = \left(\dfrac{k \cdot w_3}{w_1 w_2 w_3}\right)^2 \end{cases} \tag{10}$$

where k is a proportional coefficient. The solution of this system is a point, which is a common point passing through three circles, centered on p_1, p_2 and p_3.

The explicit solution of (10) is as below:

$$x_0 = -\frac{3}{12} r(2w_1^2 - w_2^2 - w_3^2)\Omega \tag{11}$$

$$y_0 = -\frac{\sqrt{3}}{4} r(w_3^2 - w_3^2)\Omega \tag{12}$$

$$k = \frac{\sqrt{6}}{2} r w_1 w_2 w_3 \sqrt{\Omega} \tag{13}$$

where ξ, ψ, ζ and Ω are auxiliary variables, defined as below:

$$\xi = \sqrt{(w_1 + w_2 - w_3)(w_1 + w_3 - w_2)(w_2 + w_3 - w_1)(w_1 + w_2 + w_3)} \tag{14}$$

$$\psi = w_1^4 + w_2^4 + w_3^4 - w_1^2 w_2^2 - w_1^2 w_3^2 - w_2^2 w_3^2 \tag{15}$$

$$\zeta = w_1^2 + w_2^2 + w_3^2 \tag{16}$$

$$\Omega = \frac{\zeta + \sqrt{3}\xi}{\psi} \tag{17}$$

As w_i cannot have different directions, the constraints introduced by (14) are as follows:

$$\begin{aligned} w_1 + w_2 - w_3 &\geq 0 \\ w_1 + w_3 - w_2 &\geq 0 \\ w_2 + w_3 - w_1 &\geq 0 \\ w_1 + w_2 + w_3 &\geq 0 \end{aligned} \tag{18}$$

The plots of (11) and (12), for $w_1 = 2$, are brought in Fig. 3.

Accuracy of (10) is examined by putting calculated x_0 and y_0, which came from (11) and (12), and w_i, in Eq. (5), constructing three individual equations. It shows an acceptable error in x_0 and y_0.

Fig. 4a illustrates the system along with showing several states of p_0, as $w_1 = 0.5$, $w_2 = 0.25$ and w_3 varies from 0.255 to 0.745 with step of 0.005. Fig. 4b also illustrates the system with $w_1 = 0.5$, $w_2 = 1.75$ and w_3 varies from 1.255 to 2.245 with step of 0.05.

The rotation point, $p_0(x_0, y_0)$, is evaluated using system of Eq. (10) resulting x_0 and y_0 within Eqs. (11) and (12), respectively. Further, the Climax's dominant equations of motion can be evaluated through relations below referring to Figs. 5 and 6.

The longitudinal slip of the tire is defined as a difference between the tire tangential speed and the speed of the axle relative to the road, which is represented by the following equation:

$$S_i = \begin{cases} \dfrac{V_{x'i} - R\omega_{wi}}{V_{x'i}}, & V_{x'i} > R\omega_{wi} \\ \dfrac{R\omega_{wi} - V_{x'i}}{R\omega_{wi}}, & R\omega_{wi} > V_{x'i} \end{cases} \tag{19}$$

where S_i is the longitudinal slip in the ith wheel, $V_{x'i}$ the speed of the axle in the ith wheel (Fig. 6b), ω_{wi} the angular velocity in the ith wheel and R is the radius of the wheel. The value of the longitudinal slip is limited such that $0 < |S| < 1$; in pure rolling motion $S = 0$ and in pure slipping motion $S = 1$. The former is ideal form of

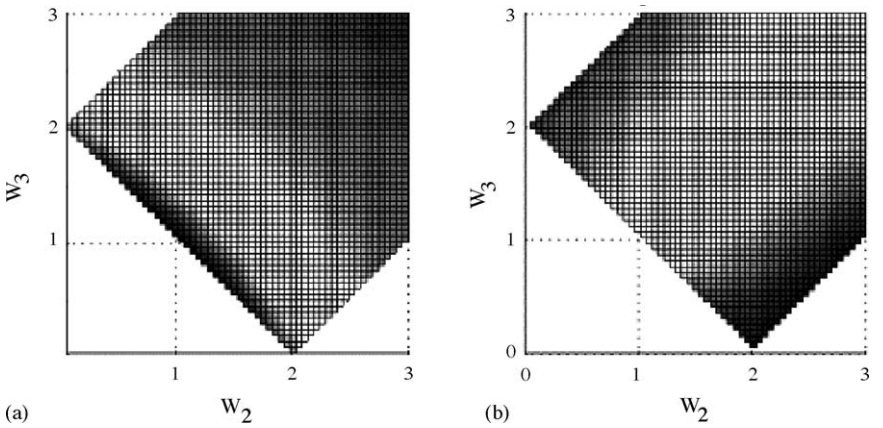

Fig. 3. Plot of the explicit solution of (10), for x_0 and y_0, respectively.

the motion which is a spin turn around the CG point. To keep track of the robot, the latter should be avoided. In actual conditions, S should lie between these two values.

Slip angle is the angle between the wheel direction and the velocity vector on the wheel defined as

$$\alpha_i = \tan^{-1}\left(\frac{V_{x'i}}{V_{y'i}}\right) \tag{20}$$

where $V_{x'i}$ and $V_{y'i}$ are the speed of the axle and the sideslip velocity, respectively. The value of the slip angle is limited such that $|\alpha| < 90^\circ$. Having V_x, V_y and ω in every moments, the velocity vector for each wheel can be derived. Further, it is possible to calculate $V_{x'i}$ and $V_{y'i}$ using equation below:

$$\begin{aligned}\vec{V}_i &= (V_x + r_i\omega\,\sin\theta_i)\hat{e}_x + (V_y + r_i\omega\,\cos\theta_i)\hat{e}_y \\ &= V_{x'i}\hat{e}_{x'i} + V_{y'i}\hat{e}_{y'i}\end{aligned} \tag{21}$$

where $\vec{V}_i$ is the velocity vector on the ith wheel, V_x and V_y the velocity of the center of mass in x and y directions, r_i the distance of the ith wheel from the center of the robot and θ_i is the direction angle of the ith wheel (Fig. 6a).

The longitudinal and lateral forces generated by a wheel are a function of the slip angle, longitudinal slip and gravitational forces. That is

$$\frac{F_{x'i}}{\mu F_{zi}} = f_x(\alpha_i, S_i) \tag{22}$$

$$\frac{F_{y'i}}{\mu F_{zi}} = f_y(\alpha_i, S_i) \tag{23}$$

where μ, F_{zi}, α_i and S_i are kinetic coefficient of friction, gravitational force (equal to $mg/3$ for each wheel due to geometric symmetry of the robot), slip angle and longitudinal slip, respectively. $F_{x'i}$ and $F_{y'i}$ are slipping

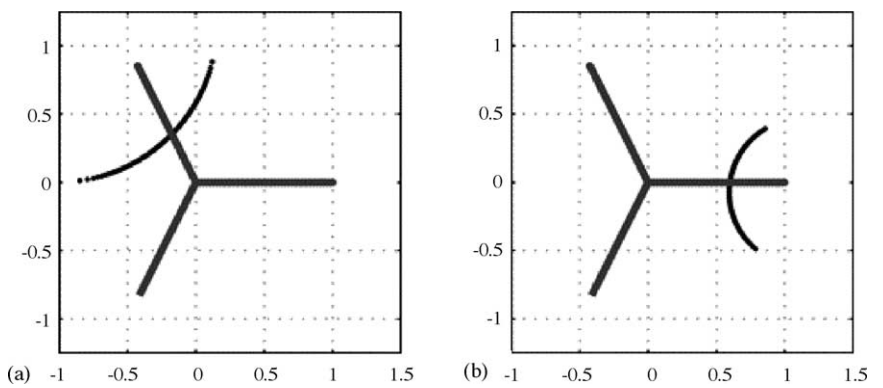

Fig. 4. p_0's due to two different setups. It is supposed that $r = 1$.

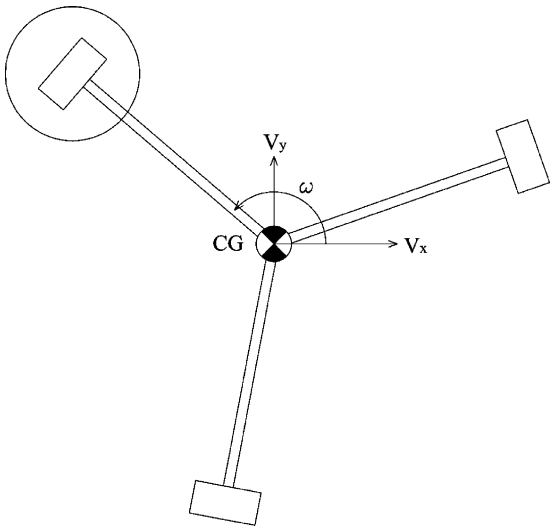

Fig. 5. Schematic of Climax, showing the wheels along with the axles placed in 120°. The area within the circle is emphasised in Fig. 6.

and rolling friction forces, respectively (Fig. 6c), which will be discussed later in Section 3.2. μ is a function of materials, nature of contacting surfaces and the relative velocity. Hence, for assuring the possibility of motion, it is essential to satisfy the following equations:

$$\mu f_x > \mu_{\text{static}} \tag{24}$$

$$\mu f_y > \mu_{\text{static}} \tag{25}$$

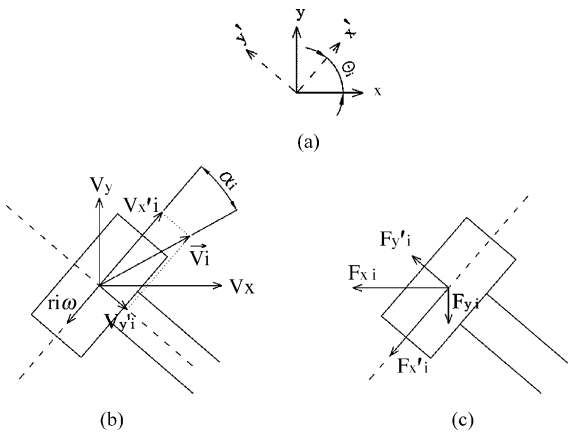

Fig. 6. (a) The original coordinates O–xy with the rotated coordinates O–$x'y'$; (b) the axle's speed $\vec{V}_i$ of wheel I; (c) the corresponding applied force F_i on wheel i.

in which μ_{static} is the static coefficient of friction. Functions f_x and f_y depend on contact patch, tread width and wheel hardness and their corresponding relations can be found in reference [36].

It should be noted that in every wheel, there is a moment about the z-axis which is negligible in comparison with values of the forces. The mentioned force is not shown in Fig. 5. The projection of forces in the above equations in x–y direction yields:

$$F_{xi} = F_{x'i} \cos\theta_i + F_{y'i} \sin\theta_i \tag{26}$$

$$F_{yi} = F_{x'i} \sin\theta_i + F_{y'i} \cos\theta_i \tag{27}$$

Now, from the Newton's second law and its generalization, we can write

$$\vec{F} = F_x \hat{e}_x + F_y \hat{e}_y \tag{28}$$

$$F_x = \sum_{i=1}^{3} F_{xi} = m(\dot{V}_x - \omega V_y) \tag{29}$$

$$F_y = \sum_{i=1}^{3} F_{yi} = m(\dot{V}_y + \omega V_x) \tag{30}$$

where $\hat{e}_x$ and $\hat{e}_y$ are unit vectors in x and y directions, respectively, and

$$M_z = \sum_{i=1}^{3} F_{x'i} r_i = I\dot{\omega} \tag{31}$$

where M_z is the summation of moments around the CG, m the mass of the Climax and I is the moment of inertia about the z-axis. It should be noted that the acceleration terms in the first two equations have two parts. The first part is related to the linear acceleration and the second part, including ω, is associated with Coriolis acceleration.

3.1. System transition from O_m–X_mY_m to absolute coordinates

As we have used a special case of alignment of the robot, in O_m–X_mY_m coordinates, we should use a transfer function to convert the system to our special alignment structure.

Consider that the mobile robot be a rigid moving on the workspace. It is assumed that the absolute coordinate system, O_w–X_wY_w, is fixed on the plane, on the

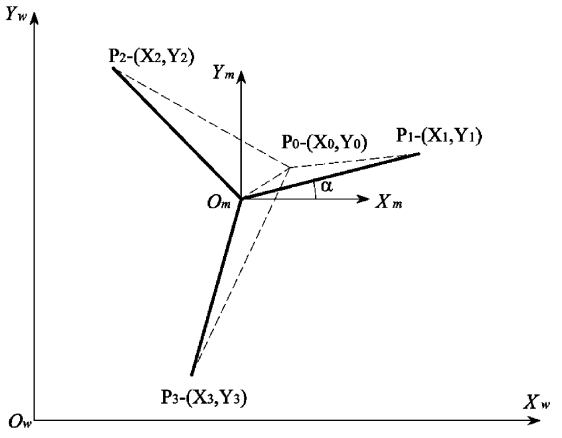

Fig. 7. Absolute coordinates O_w along with O_m and the robot.

center point of the robot at the beginning of the travel, and the moving coordinate system, O_m–X_mY_m, is fixed on the center point of the robot, parallel to O_w–X_wY_w, following movements of the robot, as shown in Fig. 7. We can use the equation below for transferring a point from the O_m–X_mY_m coordinates to the O_w–X_wY_w coordinates:

$$\begin{bmatrix} P_x \\ P_y \end{bmatrix} = \begin{bmatrix} p_x \\ p_y \end{bmatrix} + \begin{bmatrix} O_{mx} \\ O_{my} \end{bmatrix} \tag{32}$$

where p and P refer to the points measured in O_m–X_mY_m and O_w–X_wY_w coordinates, respectively.

In our notation, we use capital letters for the locations of points measured in O_w–X_wY_w coordinates, and small letters for the locations of points measured in O_m–X_mY_m coordinates.

Now, we use a rotation matrix to rotate the system to our special alignment in O_m–X_mY_m, as below:

$$\begin{bmatrix} x_i \\ y_i \end{bmatrix} = \begin{bmatrix} \cos\alpha & \sin\alpha \\ -\sin\alpha & \cos\alpha \end{bmatrix} \begin{bmatrix} x'_i \\ y'_i \end{bmatrix} \tag{33}$$

where α is the angle between $\vec{v}_1$ and the X_m axis, as shown in Fig. 7. So

$$\cos\alpha = \frac{x'_1}{\sqrt{(x'_1)^2 + (y'_1)^2}} \tag{34}$$

$$\sin\alpha = \frac{y'_1}{\sqrt{(x'_1)^2 + (y'_1)^2}} \tag{35}$$

We can evaluate the resultant instantaneous center of zero velocity, $p'_0(x'_0, y'_0)$, by the equation below:

$$\begin{bmatrix} x'_0 \\ y'_0 \end{bmatrix} = \begin{bmatrix} \cos\alpha & -\sin\alpha \\ \sin\alpha & \cos\alpha \end{bmatrix} \begin{bmatrix} x_0 \\ y_0 \end{bmatrix} \tag{36}$$

p'_0, also, can be measured in O_w–X_wY_w by Eq. (32). So the instantaneous center of zero velocity in O_w–X_wY_w coordinates can be evaluated. In O_w–X_wY_w, all primed variables are the same with nonprimed relative variables, as primed variables have no particular meaning. Therefore, P'_0 is identical to P_0.

By having P_0 in hand, the transition of the whole system can be achieved by equation below:

$$\begin{bmatrix} X_i \\ Y_i \end{bmatrix} \leftarrow \begin{bmatrix} \cos\delta & -\sin\delta \\ \sin\delta & \cos\delta \end{bmatrix} \begin{bmatrix} X_i - X_0 \\ Y_i - Y_0 \end{bmatrix} + \begin{bmatrix} X_0 \\ Y_0 \end{bmatrix} \tag{37}$$

where δ is the instantaneous rotation angle of the robot in a very short time, Δt. δ can be evaluated as below:

$$w_1 = (2\pi \cdot r_w) W_1 \tag{38}$$

$$\Delta l = \frac{\Delta t \cdot w_1}{60} \tag{39}$$

$$r_1 = \sqrt{(x_0 - x_1)^2 + (y_0 + y_1)^2} \tag{40}$$

$$\delta = \frac{180\,\Delta l}{\pi r_1} \tag{41}$$

where W_1 is the angular velocity of wheel 1 and r_w is the radius of wheels.

We can use the equation below for obtaining the location of O_m from P_i:

$$\begin{bmatrix} O_{mx} \\ O_{my} \end{bmatrix} = \frac{1}{3} \begin{bmatrix} X_1 + X_2 + X_3 \\ Y_1 + Y_2 + Y_3 \end{bmatrix} \tag{42}$$

and for calculating p'_i, we use the following equation:

$$\begin{bmatrix} p'_{ix} \\ p'_{iy} \end{bmatrix} = \begin{bmatrix} O_{mx} \\ O_{my} \end{bmatrix} - \begin{bmatrix} P_{ix} \\ P_{iy} \end{bmatrix} \tag{43}$$

3.2. Friction forces analysis

Up to now, we have considered each wheel as an individual element in the system. Now, we want to discuss the friction forces of the wheels and the effects of the wheels' forces on each other.

Equations below are used for evaluating slipping and rolling friction forces:

$$F_s = \eta_s mg \tag{44}$$

$$F_r = \eta_r mg \tag{45}$$

where F_s and F_r are slipping and rolling friction forces, respectively. η_s and η_r are slipping and rolling friction coefficients, respectively, which depend on several factors, such as velocity, materials and forms of contacting surfaces. Typically, finding the relations between mentioned factors, and η_s and η_r coefficients is mostly based on practical experiences. As a rule of thumb, we can assign a number to each of them. Equations below are a reasonable approximation for slipping and rolling friction forces in our system:

$$f_{si} = \mu_s m_w g \tag{46}$$

$$f_{ri} = \mu_r m_w g \tag{47}$$

$$m_w g = \frac{1}{3} mg \tag{48}$$

where μ_s and μ_r are constant slipping and rolling friction coefficients, respectively, and $m_w g$ is the weight force acting on each wheel. As the robot is in a geometrical symmetry, $m_w g$ is one-third of the robot weight, mg (Eq. (48)). Experimental results show that equating μ_s and μ_r with 0.3 and 0.1, respectively, provides a good approximation of the system's response [36,37]. Friction force vectors are shown in Fig. 8. As shown, slipping friction forces are along with the axis of the wheels, and rolling friction forces are perpendicular to the axis of the wheels and parallel to the surface of the movement and its direction is contrary to the rotation of the heading of the robot.

In addition to calculating the friction forces for each wheel, we should consider the effects of the wheels on each other. We have two pairs of forces, the slipping and rolling friction forces of the other two wheels, say wheels 1 and 3, that affect each wheel, say wheel 2. The effects of wheels 1 and 3 on wheel 2 are shown in Fig. 9. The superposition of these four forces and its own friction forces on each wheel, F_i, can be decomposed into two vectors along and perpendicular to the axis of the wheel. The acting vector that is along with the axis of the wheel, F_{in}, and the acting vector that is perpendicular to the axis of the wheel, F_{it}, should not exceed the slipping friction force, in order to not push

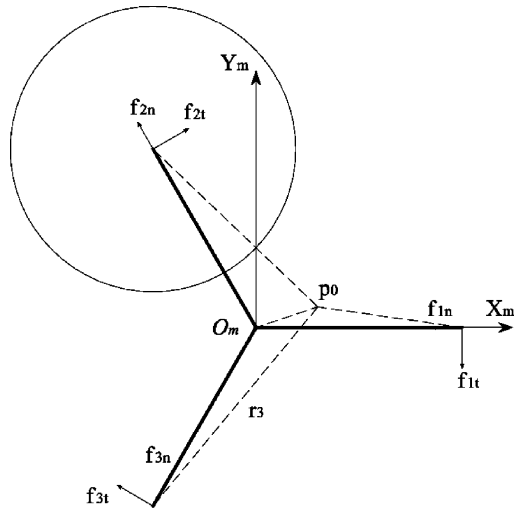

Fig. 8. Slipping and rolling friction forces of wheels. The area within the circle is emphasised in Fig. 9.

or pull the wheel aside along or perpendicular to the axis of the wheel, respectively.

The affected force, for all the wheels, F_i, can be calculated as below:

$$\vec{f}_{s1} = -\mu_s mg\hat{x} \tag{49}$$

$$\vec{f}_{r1} = -\mu_r mg\hat{y} \tag{50}$$

$$\vec{f}_{s2} = \frac{1}{2}\mu_s mg\hat{x} + \frac{\sqrt{3}}{2}\mu_s mg\hat{y} \tag{51}$$

$$\vec{f}_{r2} = \frac{-\sqrt{3}}{2}\mu_r mg\hat{x} + \frac{1}{2}\mu_r mg\hat{y} \tag{52}$$

$$\vec{f}_{s3} = \frac{-1}{2}\mu_s mg\hat{x} + \frac{\sqrt{3}}{2}\mu_s mg\hat{y} \tag{53}$$

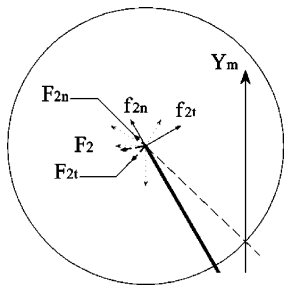

Fig. 9. The impact of friction forces of wheels 1 and 3 on wheel 2.

$$\vec{f}_{r3} = \frac{\sqrt{3}}{2}\mu_r mg\hat{x} - \frac{1}{2}\mu_r mg\hat{y} \quad (54)$$

$$\vec{F}_i = \vec{f}_{s1} + \vec{f}_{r1} + \vec{f}_{s2} + \vec{f}_{r2} + \vec{f}_{s3} + \vec{f}_{r3}. \quad (55)$$

Now, we should decompose $\vec{F}_i$ into two vectors, along and perpendicular to the vector connecting P_0 to P_i. We, for instance, evaluate $\vec{F}_{it}$ and $\vec{F}_{in}$ for wheel 2, as below:

$$R_2 = \sqrt{\left(X_0 + \frac{1}{2}\right)^2 + \left(Y_0 - \frac{\sqrt{3}}{2}\right)^2} \quad (56)$$

$$\vec{F}_{2n} = mg(\mu_r \sin\varepsilon - \mu_s \cos\varepsilon)(\cos\varepsilon \cdot \hat{x} - \sin\varepsilon \cdot \hat{y}) \quad (57)$$

$$\vec{F}_{2t} = mg(\mu_r \sin\varepsilon + \mu_s \cos\varepsilon)(-\cos\varepsilon \cdot \hat{x} - \sin\varepsilon \cdot \hat{y}) \quad (58)$$

As we examined the F_{2n} and F_{2t} forces with different points of P_0, we find that the maximum of these two vectors will not exceed the slipping friction force. So the system will remain stable for all valid points of P_0. Using Eqs. (24) and (25), and, for instance, Eqs. (57) and (58), we have shown experimentally that Climax can have full motion capabilities for conventional indoor applications.

4. Control strategy

We have evaluated the relation between w_i and instantaneous center of zero velocity, P_0, through (10). We can calculate all the w_i, surely, with having (X_0, Y_0) and one wheel's angular velocity predefined. Therefore, it is possible to achieve any desired instantaneous center of zero velocity, (X_0, Y_0), as long as constraints (18) are not violated. Hence, there are several styles of movements from beginning to destination.

To simplify the trajectory planning, our approach is based on having all the wheels to rotate with equal angular velocities or holding one wheel steady while the other two wheels have an equal angular velocity. This method has several advantages such as:

1. Simple repeated sequential motions to steer the robot from the beginning to destination.
2. No need to evaluate the system of Eq. (10), because the resultant rotation point (X_0, Y_0) is obviously placed either on center point of the robot, or on the contacting point of the steady wheel.
3. Having full motion capability, with mono-directional motor driving.

More discussion on how the motors are drove through some examples is given in the next section.

5. Experimental results

In this section, the validity of the model is checked by comparing trajectories found by experiment with those predicted by integrating the model for a series of setups. The calculations are done by a low-order numerical integrator in MATLAB 12 using a time step 0.01 s. The experimental setup parameters are shown in Table 1.

For several missions, the experimental results agree well with those of the model. In each case, the experimental trajectory follows the predicted one within a reasonable accuracy. The following are several issues of experimental results, containing spin turn with instantaneous center of zero velocity positioned on and out of the center of the robot, simple direct path traveling and crank motion. In each part, the desired path, the traveled path along with a sketch of how the motors are drove, are given.

5.1. Spin turn

Fig. 10a and b shows two different rotary motions of the robot with instantaneous center of zero velocity placed on two different points. The instantaneous center of zero velocity for Fig. 10a is placed on wheel 3. The corresponding motor driving tim-

Table 1
Experimental setup for Climax

Variable	Quantity
Radius of wheels (cm)	4.25
Distance of center of the robot to contacting point of wheels (cm)	9
Maximum speed of motors (r/s)	1.75
Maximum speed of robot's rotation (r/s)	1.85
Robot's weight (kg)	1.650

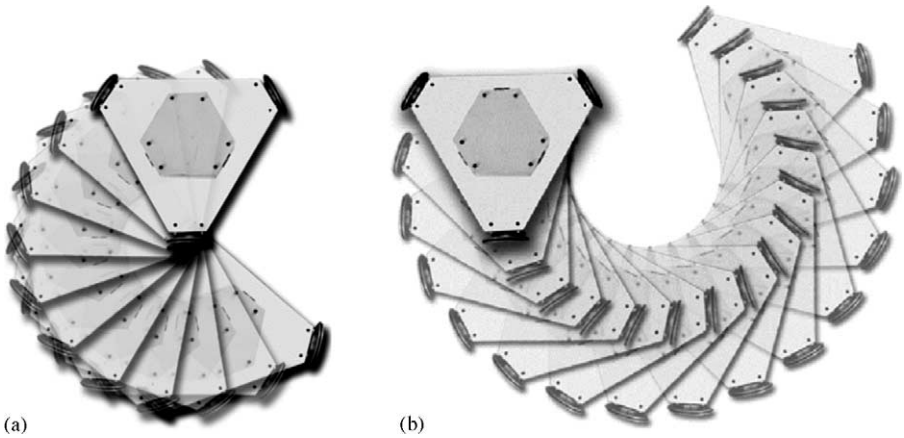

Fig. 10. Spiral motion.

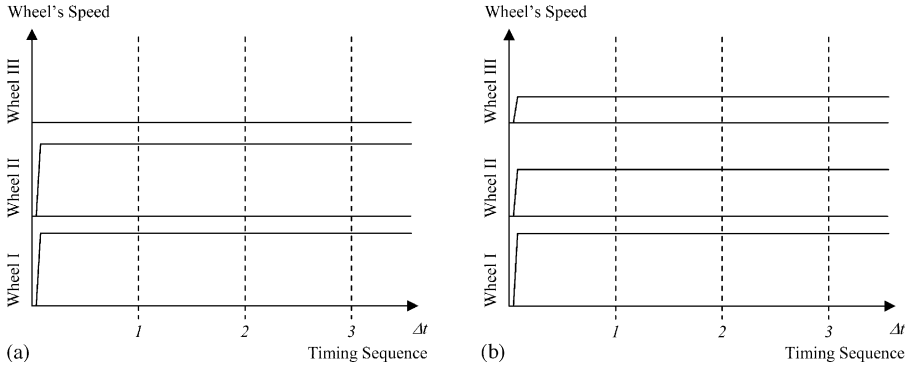

Fig. 11. Spiral motion; motor driving timing diagram.

ing diagrams are shown in Fig. 11. In this experiment, the traveled path followed the desired path. The spiral motion is an example showing the capability of the robot to rotate along a center, and does not follow the motion technique introduced in Section 4.

5.2. Direct path traveling

A direct path traveling is performed (Fig. 12). The robot traveled the path by rotating to the target, proposing the previous discussed motion planning, which is discussed in Section 4. Fig. 13 shows the robot's driftage from the desired path. It is expected as the robot should have a rotary motion to the target. The corresponding motor driving timing diagram is shown in Fig. 14.

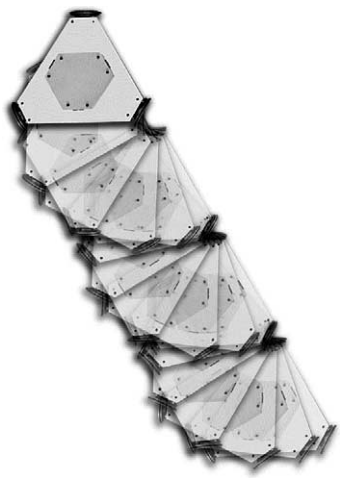

Fig. 12. Direct movement.

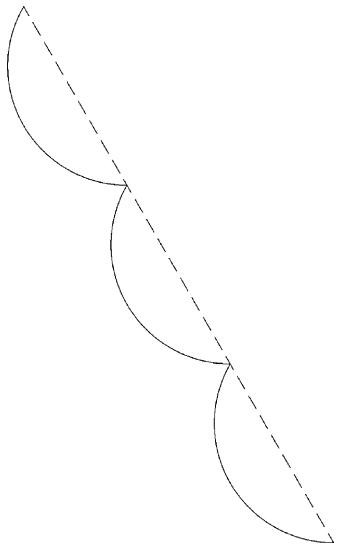

Fig. 13. Comparison between the desired path (dashed line) and the traveled path (solid curve).

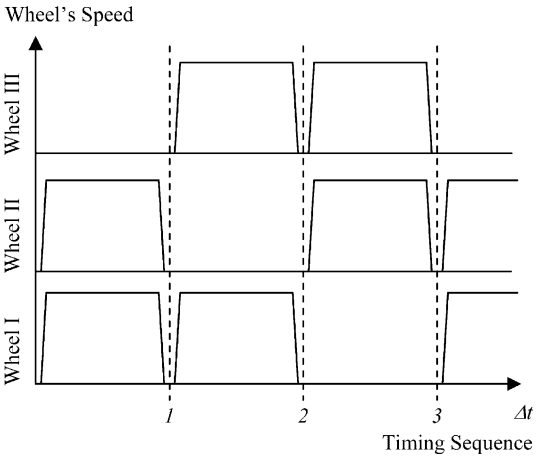

Fig. 14. Direct movement; motor driving timing diagram.

5.3. Crank motion

Fig. 15 shows a crank motion containing two different motions. As shown in Fig. 16, the robot followed the desired path in a reasonable accuracy. It is good to mention that though the robot had some deviation from the desired path through the traveling, it reached the destination point. The corresponding motor driving timing diagram is shown in Fig. 17. As shown, though the control strategy is followed, the difference of the timing interval in the third part of the diagram makes the robot to rotate. It is the point which makes the motion planning relatively easy.

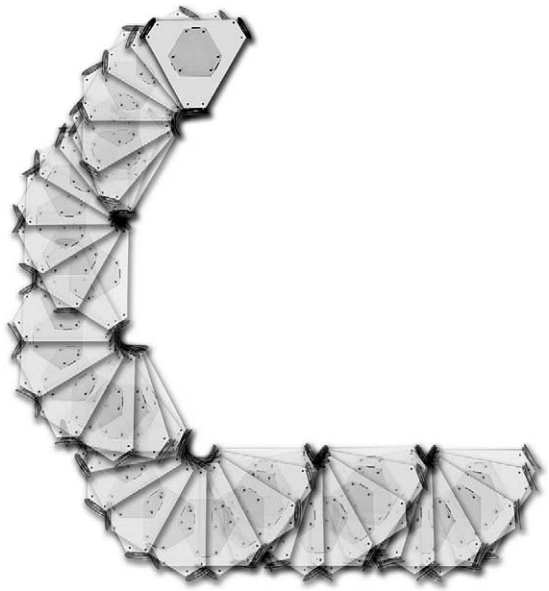

Fig. 15. Crank motion.

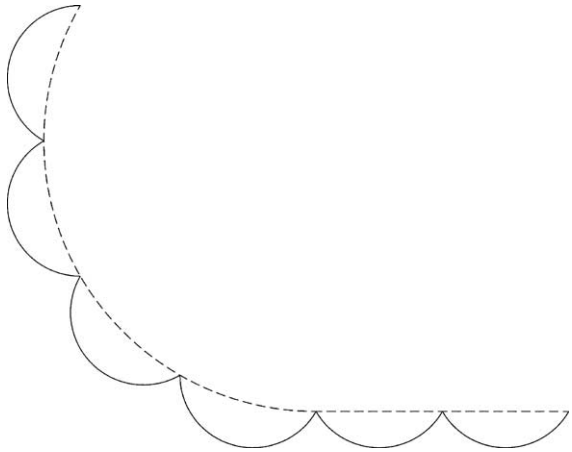

Fig. 16. Comparison between the desired path (dashed curve) and the traveled path (solid curve).

6. Sensory interpretation

To show one advantages of spiral motion, we ran an experiment using three distance-meter sensors mounted on our robot, as shown in Fig. 18.

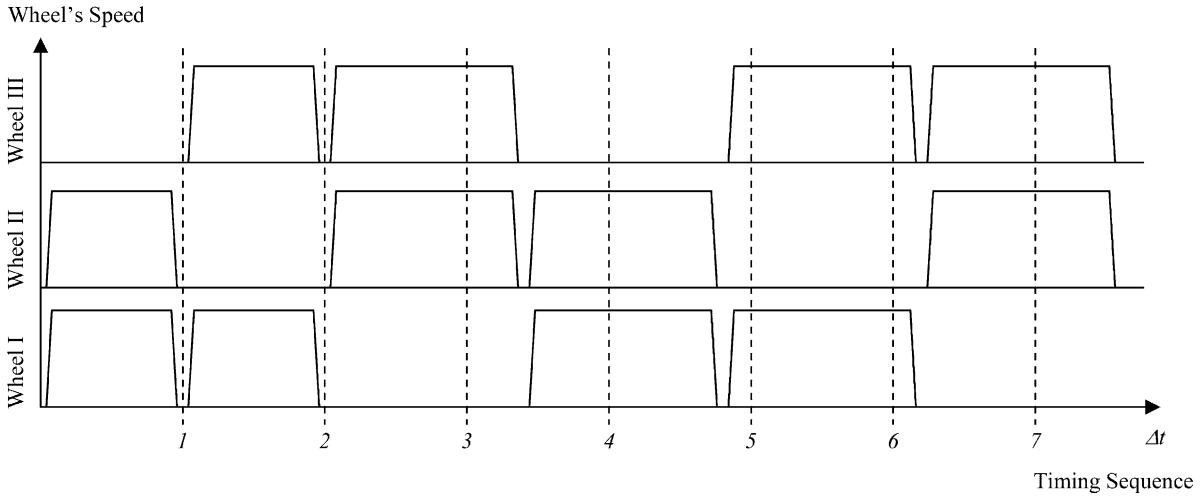

Fig. 17. Crank motion; motor control timing diagram.

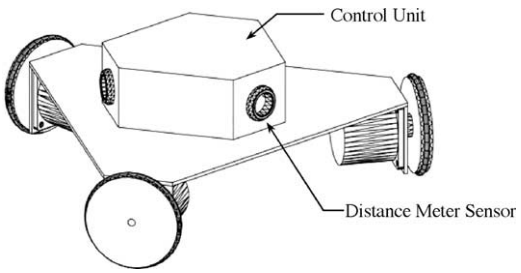

Fig. 18. The prototype of Climax.

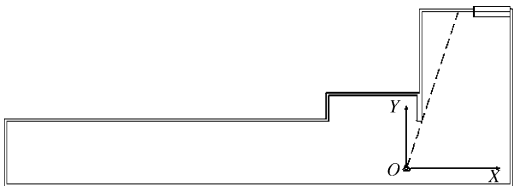

Fig. 19. Map of the corridor for experimental sensory information interpretation.

Fig. 19 shows the map of a corridor, along with the robot, which is placed somewhere in it. Fig. 20 shows a 360° view of the corridor from where the robot is located. A camera was mounted on the robot to show the site view of the robot. Fig. 21 shows the signals gathered from one of the distance-meter sensors, when the robot rotates in its place from 270° to −90° clockwise. Constructing the map from the sensory information using geometrical relations is as below:

$$P_x = l \cos\varphi \tag{59}$$

$$P_y = l \sin\varphi \tag{60}$$

where $P(P_x, P_y)$ is any intended point and φ is the angle between the sensor and X_m in O_m–X_mY_m coordinates.

Though interpretation of distance-meter sensor information is handy and simple, it is so effective in map construction. The map represented by robot, through considering the sensory information, is shown in Fig. 22. The discontinuity in Fig. 22 is indicated in Fig. 21 with an arrow.

Fig. 20. 360° view of the corridor.

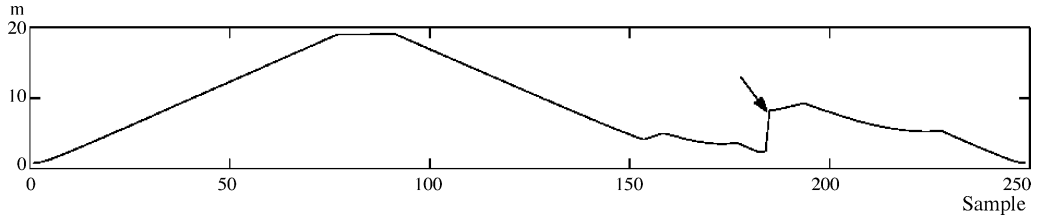

Fig. 21. Sensory information gathered from the distance-meter sensor, which is mounted on the robot. Arrow shows the discontinuity point.

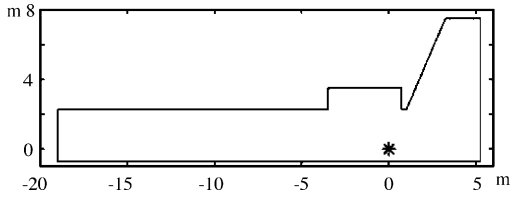

Fig. 22. Map representation due to sensory information. Asterisk shows the robot's position.

7. Conclusion

An autonomous tri-wheel spiral robot was designed and built. The mathematical model of the robot and an algorithm for motion planning were developed. The model was validated through a set of experiments. Simulation and experimental trajectories of the robot on the plane were found to agree to a reasonable accuracy. As compared to existing motion planners, most of which require intensive numerical computation, our strategy involves simple algorithmic iterative motion and provides the scope for easy implementation. This study demonstrates the feasibility of the idea and we expect to improve its design in future.

Acknowledgements

The support of the Azad University of Qazvin is gratefully acknowledged. Thanks also to Aidin Delnavaz for his hints on dynamic analysis of the robot, and thanks to Mohammad Chitsazan for his assistance building the robot and also thanks to Ali Rahmani for taking and preparing the photos.

References

[1] P.F. Muir, C.P. Neuman, Kinematic modeling of wheeled mobile robots, J. Rob. Syst. 4 (1987) 281–340.
[2] J.P. Laumond, Feasible trajectories for mobile robots with kinematic and environment constraints, in: Proceedings of the International Conference on Intelligent Autonomous Systems, 1986.
[3] F.G. Pin, H.A. Vasseur, Trajectory generation for autonomous mobile robots with non-holonomic and steering angle constraints, in: Proceedings of the IEEE International Workshop on Intelligent Motion Control, 1990, pp. 295–299.
[4] H.A. Vasseur, F.G. Pin, J.R. Taylor, Navigation of a car-like mobile robot in obstructed environments using convex polygonal cells, Rob. Autonomous Syst. 10 (2–3) (1992) 133–146.
[5] J. Ostrowski, A. Lewis, R. Murray, J. Burdick, Nonholonomic mechanics and locomotion: the snake board example, in: Proceedings of ICRA'94, 1994, pp. 2391–2397.
[6] R.M. Murray, S.S. Sastry, Nonholonomic motion planning: steering using sinusoids, IEEE Trans. Autom. Control 38 (May (5)) (1993) 700–716.
[7] O.J. Sordalen, Y. Nakamura, Design of a nonholonomic manipulator, in: Proceedings of ICRA'94, 1994, pp. 8–13.
[8] A. Bicchi, R. Sorrentino, Dexterous manipulation through rolling, in: Proceedings of ICRA'95, 1995, pp. 452–457.
[9] A. De Luca, R. Mattone, G. Oriolo, Dynamic mobility of redundant robots using end-effector commands, in: Proceedings of ICRA'96, 1996.
[10] V. Jurdjevic, The geometry of the plate-ball problem, Arch. Ration. Mech. Anal. 124 (1993) 305–328.
[11] G. Lafferriere, H. Sussmann, A differential geometric approach to motion planning, in: Z. Li, J.F. Canny (Eds.), Nonholonomic Motion Planning, Kluwer, Norwell, MA, 1993, pp. 234–270.
[12] J.P. Laumond, Nonholonomic motion planning for robots, in: Proceedings of ICRA'98, Tutorial Notes, 1998.
[13] R. Mukherjee, B. Emond, J.L. Junkins, Optimal trajectory planning for mobile robots using Jacobian elliptic functions, Int. J. Rob. 16 (6) (1997) 826–839.
[14] R.R. Murray, Z. Li, S.S. Sastry, A Mathematical Introduction to Robotic Manipulation, CRC Press, Boca Raton, FL, 1993.
[15] K. Watanabe, Control of an omnidirectional mobile robot, in: Proceedings of Second International Conference on Knowledge-Based Intelligent Electronic Systems, April 1998, pp. 51–60.
[16] M. Wada, S. Mori, Modeling and control of a new type of omnidirectional holonomic vehicle, in: Proceedings of AMC'96, 1996, pp. 265–270.
[17] H. Asama, et al., Development of an monodirectional mobile robot with 3 DOF decoupling mechanism, in: Proceedings of ICRA'95, May 1995, pp. 1925–1930.

[18] F.G. Pin, S.M. Killough, A new family of omnidirectional and holonomic wheeled platforms for mobile robots, Proc. IEEE Trans. Rob. Autom. 10 (4) (1994) 480–489.
[19] M. West, H. Asada, Design and control of ball wheel omnidirectional vehicles, in: Proceedings of ICRA'95, May 1995, pp. 1931–1938.
[20] Y. Kanayama, B.I. Hartman, Smooth local path planning for autonomous vehicles, in: Proceedings of ICRA'89, 1989, pp. 1265–1270.
[21] F.G. Pin, M. Beckerman, P.F. Spelt, J.T. Robinson, C.R. Weisbin, Autonomous mobile robot research using the HERMIES-III robot, in: Proceedings of IROS'89, 1989, pp. 251–256.
[22] R.A. Brooks, Elephants don't play chess, Rob. Autonomous Syst. 6 (1–2) (1990) 3–15.
[23] R.C. Arkin, Integrating behavioral, perceptual, and world knowledge in reactive navigation, Rob. Autonomous Syst. 6 (1–2) (1990) 105–122.
[24] Y. Koren, J. Borenstein, Potential field methods and their inherent limitations for mobile robot navigation, in: Proceedings of ICRA'93, 1993, pp. 1398–1404.
[25] S. Halme, T. Schonberg, Y. Wang, Motion control of a spherical mobile robot, in: Proceedings of AMC'96, 1996, pp. 259–264.
[26] A. Bicchi, A. Balluchi, D. Prattichizzo, A. Gorelli, Introducing the sphericle: an experimental testbed for research and teaching in nonholonomy, in: Proceedings of ICRA'97, 1997.
[27] S. Bhattacharya, S.K. Agrawal, Spherical rolling robot: a design and motion planning studies, in: Proceedings of ICRA'2000, 2000.
[28] R. Mukherjee, M.A. Minor, J.T. Pukrushpan, Simple motion planning strategies for Spherobot: a spherical mobile robot, in: Proceedings of IEEE International Conference on Decision and Control, 1999, pp. 2132–2137.
[29] A.H. Javadi, P. Mojabi, Introducing August: a novel strategy for an omnidirectional rolling robot, in: Proceedings of ICRA'02, 2002.
[30] L. Ferriere, B. Raucent, G. Campion, Design of omnimobile robot wheels, in: Proceedings of ICRA'96, 1996, pp. 3664–3670.
[31] J. Tang, K. Watanabe, Y. Shiraishi, Design and traveling experiment of an omnidirectional holonomic mobile robot, in: Proceedings of IEEE International Conference on Intelligent Robots and Systems, 1996, pp. 66–73.
[32] E. Nakano, N. Koyachi, An advanced mechanism of the omnidirectional vehicle (ODV) and its application to the working wheelchair for the disabled, in: Proceedings of IEEE International Conference on Advanced Robotics, 1983, pp. 277–284.
[33] P.F. Muir, C.P. Neuman, Kinematic modeling of wheeled mobile robots, J. Rob. Syst. 4 (1987) 281–340.
[34] L. Ferriere, B. Raucent, RollMOBS, a new universal wheel concept, in: Proceedings of ICRA'98, 1998, pp. 1877–1882.
[35] M. West, H. Asada, Design of a holonomic omnidirectional vehicle, in: Proceedings of ICRA'92, vol. 1, May 1992, pp. 97–103.
[36] H.T. Szostak, W.R. Allen, T.J. Rosenthal, Analytical Modeling of Driver Response in Crash Avoidance Maneuvering. An Interactive Model for Driver/Vehicle Simulation, vol. II. U.S. Department of Transportation Report, NHTSA DOT HS-807-271, April 1988.
[37] H.B. Pacejka, E. Bakker, Magic formula tyre model, Vehicle Syst. Dyn. 21 (1993) 1–18.

Amir Homayoun Javadi was born in Tehran, Iran, in 1980. He finished his high-school in National Organization for Development of Exceptional Talents, Qazvin, Iran, in 1998. He received his BSc in electronics engineering from Azad University of Qazvin, Iran, in 2003, and currently he is pursuing MSc degree on mechatronics engineering at Azad University of Qazvin, Iran. He has published over 20 articles in international conferences, over 20 articles in Iranian conferences and some articles in international journals. His current research interests include mobile robots, multi-agent robotic environments and autonomous systems.

Puyan Mojabi was born in Qazvin, Iran, in 1980. He finished his high-school in National Organization for Development of Exceptional Talents, Qazvin, Iran, in 1998. He received his BSc in telecommunication engineering from University of Tehran, Iran, in 2002, and currently he is pursuing MSc degree on telecommunication engineering (field and waves) at Iran University of Science and Technology, Iran. He has published over 20 articles in international conferences, over 20 articles in Iranian conferences and some articles in international journals. His current research interests include mobile robots, inter-robot communication and autonomous systems.